Robotics and Autonomous Systems 95 (2017) 25–36

Contents lists available at ScienceDirect

Robotics and Autonomous Systems

journal homepage: www.elsevier.com/locate/robot

Collision-free formation and heading consensus of nonholonomic robots as a pose regulation problem

Jingfu Jin, Nicholas Gans *

Department of Electrical Engineering, University of Texas at Dallas, Richardson, TX 75080, USA

HIGHLIGHTS

- A novel, decentralized control algorithm to achieve a collision-free formation of multiple, network connected, nonholonomic mobile robots.
- Heading and formation consensus simultaneously is achieved simultaneously through a smooth control law.
- Stability analysis is established with Lyapunov analysis and Barbalat's Lemma.
- Simulations and experiments have been conducted to verify the proposed approach.

ARTICLE INFO

Article history:
Received 2 September 2015
Received in revised form 30 March 2017
Accepted 21 May 2017
Available online 27 June 2017

ABSTRACT

This paper presents a novel, decentralized control algorithm to address the problem of controlling of multiple, network connected, nonholonomic mobile robots to achieve a collision-free formation and heading consensus simultaneously. Our approach transforms the formation and heading consensus problem to a pose regulation problem. The pose is derived by a virtual graph, which is an isomorphic mapping of the graph of the network connected systems. If the system is holonomic, traditional consensus on the virtual graph can stabilize the real system to the desired formation. In the case of nonholonomic systems, such as mobile robots, each robot's pose then is regulated to the known consensus pose by a novel smooth and continuous control law. The control law also induces the real robot systems to achieve not only the desired formation but also heading consensus. We prove the proposed control schemes are globally asymptotically stable. Theoretical analysis, several simulations, and experiments have been conducted to verify the effectiveness of the proposed approach.

1. Introduction

Networked multi-robot systems allow a high degree of flexibility and adaptability [1–5]. Such systems can fulfill diverse and complex tasks efficiently and effectively, such as surveillance [6], cargo transportation, farming operations [4,5], satellite formation [7], cooperative manipulation [8] Formation control remains one of the primary and practical issues for utilizing a multi-robot systems.

Formation control of multi-robot systems has been studied through a number of approaches, including control theoretical approaches [9–14], optimization approaches such as MDP/POMDP [15,16], and planning-based methods [17–19]. In this paper, we focus on control theoretical approaches. Within this framework, there are virtual structure approaches [20–22], leader–follower approaches [10,23–25], decentralized approaches [9,26,27], and more. The merit of virtual structure and leader–follower approaches is the simplicity of the controller design. However, a drawback of these two approaches is that they are frail to external forces. Moreover, the communication bandwidth may also be an issue for a large number of robots.

Decentralized approaches allow each robot to make its own decision. One decentralized approach is consensus, in which each agent in a group is induced to converge to a common state or value using only neighbors' information [9,28,29]. Such approach is also known as nearest neighbor approach. One of the advantage of consensus-based approaches is robustness to a broad range of distribution of a group of robots. Thus, consensus-based formation control algorithm is remediable against disturbances.

The geometry of a desired formation is usually defined in terms of relative positions [14,26,30], relative bearings [31,32], relative distances [33,34], or combination of those approaches [35]. Consensus-based formation control for systems modeled by first order and second order dynamics is studied in [36,37] and [38], respectively. Compared with first and second order dynamics systems, formation control and heading consensus of multiple nonholonomic mobile robots is much harder problem since there are

* Corresponding author.
E-mail addresses: jingfu.jin@utdallas.edu (J. Jin), ngans@utdallas.edu (N. Gans).

http://dx.doi.org/10.1016/j.robot.2017.05.008
0921-8890/

no smooth, time-invariant state feedback controllers to stabilize such systems [39]. However, many of mobile robots or vehicles seen today is nonholonomic systems. Therefore, designing a novel formation and heading consensus control algorithm is necessary.

Various consensus-based control algorithms also were studied in the literature. Consensus-based formation control in $\mathbb{R}^2$ was investigated in [40] with a given desired orientation. A distributed controller is proposed with respect to a backstepping approach combining consensus algorithm and singular perturbation theory in [41]. Cascaded theories aid to transform the consensus problem of multiple nonholonomic robots into consensus problems of two simple subsystems in [42]. Moreover, flocking of a group of nonholonomic mobile robots is studied in [43,44]. To our best knowledge, there are few papers considering formation control and heading consensus for multiple nonholonomic mobile robots. One example to address this problem employed a distributed low-gain approach based on the gradient of an potential function [45]. Another example is a switched-system consensus-based attractor approach in [46].

The main contribution of this paper is a novel decentralized control algorithm designed to handle formation control, heading consensus and collision avoidance of multiple nonholonomic mobile robots **simultaneously**. Approaches such as [26,38,40] only show that the relative positions of the robots converge to the relative positions of the desired formation, but they do not achieve orientation consensus. Note that a common orientation is necessary for many tasks such as driving in formation. Our approach is also globally asymptotically stable, as it eschews potential fields or other techniques that are known to have local minima in their control laws.

The approach is inherently based on consensus algorithms [9] but transforms them into a pose regulation problem. We introduce a virtual graph that is isomorphic to the robots' communication or sensing graph. Thus, the virtual graph and the robots' communication graph share the same Laplacian and normalized Laplacian matrix. We then design a novel smooth and continuous control law to achieve consensus on the virtual graphs and show that the same control inputs applied to the real robots will induce the multiple robots system to the desired formation and heading consensus. We extended this approach to nonholonomic mobile robots and design a pose regulation controller that simultaneously achieves the formation and heading consensus while avoiding collision with other robots during motion. Note that the control law is suitable for implementation using on-board sensors and wireless communication to report each robot's pose to the neighbors. We prove the proposed control scheme is globally asymptotically stable using Lyapunov analysis and Barbalat's lemma. Through our stability analysis, we show that the robots form the desired formation with respect to a common reference, which is the average state of the initial state of the virtual robots. To verify the effectiveness of the proposed approach, numerous simulations and experiments have been conducted. Simulation and experimental results show that the proposed approach is robust under switching topologies and for switching formations.

The rest of this paper is structured as follows. Section 2 introduces background on the single-integrator dynamics system, a class of continuous and smooth saturation function, the fundamental knowledge of algebraic graph theory and consensus algorithm. Section 3 describes a novel formation and heading consensus control algorithm for multiple nonholonomic mobile robots including collision avoidance. Stability analysis is established with Lyapunov analysis and Barbalat's Lemma. Sections 4 and 5 provide simulation and experimental results that verify the proposed approach. Finally, conclusion appears in Section 6.

2. Background

2.1. Single-integrator dynamics system

Consider a system composed of N agents that are connected through a network. Denote that the state of agent i as $p_i \in \mathbb{R}^n$. Consider each agent to have single-integrator dynamics [29] given by

$$\dot{p}_i(t) = u_i(t), \quad i \in \{1, \ldots, N\} \tag{1}$$

where $u_i \in \mathbb{R}^n$ is the input vector. The collective state of the group of agents is given by $p = \left[p_1^T, p_2^T, \ldots, p_N^T\right]^T \in \mathbb{R}^{Nn}$ and the collective system dynamics yields

$$\dot{p}(t) = u(t) \tag{2}$$

where $u = \left[u_1^T, u_2^T, \ldots, u_N^T\right]^T \in \mathbb{R}^{Nn}$.

2.2. Algebraic graph theory

Graph theory is a useful tool to describe the connectivity of a network connected system such as the network topology of multi-agent system [9,28,37,47]. The network topology is modeled as a graph $G = (V, E)$, which consists of a set of vertices $V = \{v_1, v_2, \ldots, v_N\}$ and a set of corresponding edge $E = \{(i, j) \in V \times V\}$ [48]. If the pair set of edges are unordered (e.g., (i, j) & $(j, i) \in E$), then it is an undirected graph. Otherwise, it is a directed graph. Define the number of connected neighbors of the vertex i as $\deg(v_i)$. Denote $D_i = \sqrt{\deg(v_i)} \in \mathbb{R}$ and $D = \text{diag}(D_1, \ldots, D_N)$. Thus, $\Delta = D^T D$, $D = D^T$, and $\left(D^{-1}\right)^T = \left(D^T\right)^{-1}$.

In the context of an undirected graph with N vertices, the adjacency matrix $A = A(G) \in \mathbb{R}^{N\times N}$ is defined as

$$a_{i,j} = \begin{cases} 1 & \text{if } i \neq j \text{ and } (i, j) \in E \\ 0 & \text{otherwise.} \end{cases} \tag{3}$$

In addition, the degree matrix $\Delta = \Delta(G) \in \mathbb{R}^{N\times N}$ is defined as

$$\Delta_{i,j} = \begin{cases} \deg(v_i) & \text{if } i = j \\ 0 & \text{otherwise.} \end{cases} \tag{4}$$

Graph G also has an associated Laplacian matrix $L \in \mathbb{R}^{N\times N}$, which is defined as

$$L_{i,j} = \begin{cases} \deg(v_i) & \text{if } i = j \\ -1 & \text{if } i \neq j \text{ and } (i, j) \in E \\ 0 & \text{otherwise.} \end{cases} \tag{5}$$

Moreover, $L = \Delta - A$. The graph Laplacian has a number of well-known properties [26,49].

Remark 2.1 (*Well-Known Properties of Laplacian Matrix*)**.**

- $L(G)$ is symmetric and positive semi-definite.
- For the graph to be connected, at most one eigenvalue can be zero, i.e., $\lambda_1 = 0$ and $\lambda_i > 0$, $i \in \{2, \ldots, N\}$.
- The second smallest eigenvalue $\lambda_2(L)$ can indicate the connectivity of the graph. Moreover, $\text{null}(L) = \text{span}(\mathbf{1})$, where $\text{null}(\cdot)$ denotes the null space and $\mathbf{1} = [1, \ldots, 1]^T \in \mathbb{R}^N$.

The normalized Laplacian matrix $L^d \in \mathbb{R}^{N\times N}$ is defined as $L^d_{i,j} = D_i^{-1} L_{i,j} D_i^{-1}$. This gives

$$L^d = (D^{-1})^T L D^{-1} = (D^T)^{-1} L D^{-1} \tag{6}$$

and

$$L = D^T (D^T)^{-1} L D^{-1} D = D^T L^d D. \tag{7}$$

Since L is real and symmetric, it is diagonalizable. Then we can choose a proper M, orthogonal matrix such that $M^{-1} = M^T$ [49], and

$$M^T L M = \Lambda \tag{8}$$

with $\Lambda = \text{diag}(0, \lambda_2, \ldots, \lambda_N)$ the diagonal matrix containing the eigenvalues of L. Inserting (7) to (8) yields,

$$M^T L M = M^T D^T L^d D M = (DM)^T L^d (DM) = \Lambda. \tag{9}$$

The matrix transformation given by M and DM preserves the eigenvalues so that the normalized Laplacian matrix L^d has the same eigenvalues and properties as the matrix L given in Remark 2.1.

Assumption 2.1 (*Connected and Undirected Graph*)**.** Through the paper, we assume the communication or sensing graph, G, is connected and undirected such that Remark 2.1 is always true. There also exists a path connecting any two nodes and (i, j) & $(j, i) \in E$.

2.3. Graph isomorphism

Let G and G^* be two graphs. An isomorphism from G to G^* is a one-to-one mapping, that yields

$$\phi : V(G) \to V(G^*) \tag{10}$$

such that any two vertices v_i and v_j are adjacent in G if and only if vertices $\phi(v_i)$ and $\phi(v_j)$ are adjacent in G^*. Thus, G and G^* are *isomorphic graphs* if there exists an isomorphism between them [48].

2.4. Reach consensus on graph G

Consider a collection of N agents with single-integrator dynamics (2), which are interconnected via local communication or sensing graph. The network connection is modeled as a graph $G = (V, E)$, in which each agent constitutes a vertex, and an edge exists if any two agents are connected. *Consensus* is reached by the collection of N agents using if $\forall\ i, j$ and for any $p_i(0)$, $p_i(t) \to p_j(t)$ as $t \to \infty$ [29,37]. Additionally, denote $I_k \in \mathbb{R}^{k\times k}$, $k \in \mathbb{N}$ as the identity matrix, and the Kronecker product by two matrices is represented by $A \otimes B$.

The following proposition is well established, but is included here to provide background and framework for our later stability proofs.

Proposition 2.1 (*Reach Consensus Using Normalized Laplacian Matrix*)**.** *Assumption 2.1 is true. Suppose the following control input is applied to each agent*

$$\begin{aligned} u_i(t) &= D_i^{-1} \sum_{j\in\mathcal{N}_i} (p_j(t) - p_i(t)) D_i^{-1} \\ &= \left(D_i^{-1} \sum_{j\in\mathcal{N}_i} p_j(t) D_i^{-1} \right) - p_i(t). \end{aligned} \tag{11}$$

Then, the all agents will converge to a common state, which is the average of the initial state of the agents.

Proof. The closed-loop system dynamics can be written compactly with (6) as

$$\begin{aligned} \dot{p}(t) &= -\left(\left((D^{-1})^T L D^{-1} \right) \otimes I_n \right) p(t) \\ &= -(L^d \otimes I_n) p(t) \end{aligned} \tag{12}$$

where $p(t) = \left[p_1^T, p_2^T, \ldots, p_N^T \right]^T \in \mathbb{R}^{Nn}$. Moreover, only a single eigenvalue of L^d is 0, and all other eigenvalues are strictly positive.

Consider a Lyapunov function

$$V = \frac{1}{2} p^T(t) p(t) \tag{13}$$

and the time derivative of V is given by

$$\begin{aligned} \dot{V} &= p^T(t) \dot{p}(t) \\ &= -p^T(t) (L^d \otimes I_n) p(t). \end{aligned} \tag{14}$$

We conclude that $\dot{V} < 0$ whenever $p(t) \notin \text{null}(L^d \otimes I_n)$. Thus $p(t) \to \text{null}(L^d \otimes I_n)$. By LaSalle's theorem, $p_i(t) - p_j(t)$ converges to zero for all i and j if the graph is connected. ■

3. Formation control and heading consensus

The pose coordination on the domain $\mathbb{R}^2 \times \mathbb{T}$ will be addressed in this section. We propose a virtual graph of the given graph G, and each vertex of the virtual graph will be considered as a virtual nonholonomic mobile robot. We will propose a continuous and smooth control law to make the pose coordination on the virtual graph. The same control law will lead to reaching the desired formation and heading consensus simultaneously for nonholonomic mobile robots on the graph G.

3.1. Pose coordination on virtual graph G* and formation analysis on graph G

Definition 3.1 (*Desired Formation*)**.** A desired formation is specified as a set of constant translation vectors $z_i \in \mathbb{R}^n$, $i \in \{1, \ldots, N\}$ with respect to (w.r.t.) a common reference coordinate frame O; e.g., a pentagon style of desired formation is illustrated in Fig. 1(a). Note that the reference frame can be any common reference frame.

Suppose a system is composed of N agents with single integrator dynamics (2), which have the desired formation given by a set offsets $z_i \in \mathbb{R}^n$. A graph G is used to describe the network connection among the agents. A set of virtual agent is described

$$p_i^*(t) = p_i(t) + z_i \tag{15}$$

where $p_i^* \in \mathbb{R}^n$, $i \in \{1, \ldots, N\}$. The network connection of virtual agents defines a virtual graph G^*, which is an isomorphic graph of the graph G. Note that the graph G and the virtual graph G^* share the same Laplacian matrix L and normalized Laplacian L^d.

Each virtual agent's dynamics is governed by

$$\dot{p}_i^*(t) = u_i^*(t). \tag{16}$$

Since z_i is a known constant column vector, taking the time derivative of (15) yields

$$\dot{p}_i^*(t) = \dot{p}_i(t) = u_i^*(t). \tag{17}$$

To visualize the relationship between the graphs G and G^*, we give an example using a five-robot system in 2-dimensional space. The desired formation shape is a regular pentagon, and the relative translations z_i, $i \in \{1, \ldots, 5\} \in \mathbb{R}^2$ w.r.t. a reference frame O are illustrated in Fig. 1(a) and the original graph G and the virtual graph G^* are illustrated in Fig. 1(b).

Proposition 3.1. *Given Assumption 2.1, suppose the following control input is applied to each virtual agent*

$$\begin{aligned} u_i^* &= D_i^{-1} \sum_{j\in\mathcal{N}_i} (p_j^* - p_i^*) D_i^{-1} \\ &= \left(D_i^{-1} \sum_{j\in\mathcal{N}_i} p_j^* D_i^{-1} \right) - p_i^*, \end{aligned} \tag{18}$$

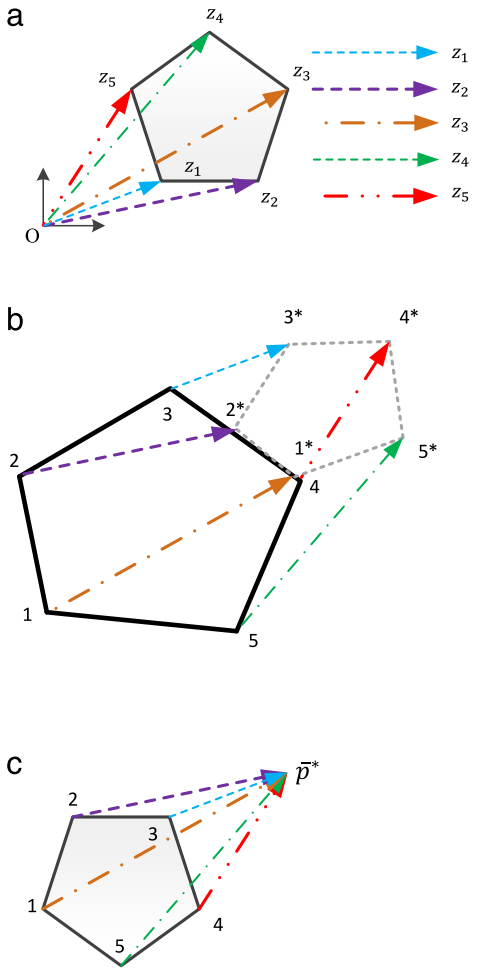

Fig. 1. (a) An example of a desired formation shape with respect to a common reference O. The arrows represent the translation vectors $z_j, j \in \{1, 2, \ldots, 5\}$. (b) The black solid-line is an original graph $G = \{1 \leftrightarrow 2 \leftrightarrow 3 \leftrightarrow 4 \leftrightarrow 5 \leftrightarrow 1\}$ and the light black dotted-line is an isomorphic (or virtual) graph $G^* = \{1^* \leftrightarrow 5^* \leftrightarrow 4^* \leftrightarrow 3^* \leftrightarrow 2^* \leftrightarrow 1^*\}$ of the graph G. (c) Virtual robots converge to a common state but the real robots converge to the desired formation about $\bar{p}^*$.

then, the virtual agents will reach a consensus, and the true agents reach the desired formation w.r.t. a common reference frame. Note that a weighted Laplacian matrix can be used to change the convergence rate of the pose consensus problem [9].

Proof. The closed-loop virtual system dynamics can be written compactly as

$$\dot{p}^* = -(L^d \otimes I_n)p^*(t) \tag{19}$$

where $u^* = \left[u_1^{*T}, u_2^{*T}, \ldots, u_N^{*T}\right]^T \in \mathbb{R}^{Nn}$ and $p^* = \left[(p_1^*)^T, (p_2^*)^T, \ldots, (p_N^*)^T\right]^T \in \mathbb{R}^{Nn}$.

According to Proposition 2.1, under the Lyapunov function

$$V = \frac{1}{2}(p^*)^T(t)p^*(t), \tag{20}$$

the virtual agents in the virtual graph will reach consensus using control law (18), and converge to the average of its initial values as [26]

$$\lim_{t\to\infty} p_i^*(t) = \frac{1}{N}\sum_{j=1}^{N} p_j^*(0) = \bar{p}^*. \tag{21}$$

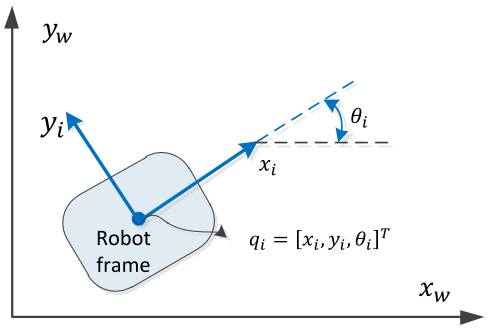

Fig. 2. The configuration for ith mobile robot.

Then, inserting Eq. (15) into (21) yields

$$\lim_{t\to\infty} p_i(t) = \bar{p}^* - z_i. \tag{22}$$

Clearly see the agent i stabilizes to a desired position w.r.t. a common reference $\bar{p}^*$. Thus, all agents on graph G will form a desired formation w.r.t. a centroid $\bar{p}^*$, and each agent will have the relative translation $z_i, i \in \{1, \ldots, N\}$ w.r.t. the centroid. In other words, the true system achieves the desired formation about the centroid by Definition 3.1. ■

Corollary 3.1 (*Equilibrium*)**.** *In term of the virtual agent p_i^* with single integrator dynamics, the equilibrium point $\left(D_i^{-1}\sum_{j\in\mathcal{N}_i} p_j^* D_i^{-1}\right)$ is in the invariant set of the Lyapunov function in (20). Therefore, stabilizing to this point means the virtual agents reached consensus, and the true agents reach the desired formation w.r.t. a common reference frame.*

3.2. Extension to Nonholonomic Mobile Robots

Consider the formation and heading consensus problem for nonholonomic mobile robots on domain $\mathbb{R}^2 \times \mathbb{T}$. Each robot can be considered as an agent or vertex on graph G. The pose of the mobile robot i w.r.t. the world coordinate frame is illustrated in Fig. 2. Let $p_i = [x_i, y_i]^T \in \mathbb{R}^2$ denote the position of the mobile robot i, which has a specific orientation $\theta_i \in \mathbb{T}$ w.r.t. the world coordinate frame. Then, the pose of the robot i is represented as $q_i = \left[p_i^T, \theta_i\right]^T \in \mathbb{R}^2 \times \mathbb{T}$. A nonholonomic mobile robot cannot move along a lateral direction due to the nonholonomic constraints $\dot{x}_i \sin(\theta_i) - \dot{y}_i \cos(\theta_i) = 0$. Hence, the motion of robot i can be described by the following nonholonomic kinematics [50]

$$\dot{q}_i(t) = \begin{bmatrix} \dot{x}_i(t) \\ \dot{y}_i(t) \\ \dot{\theta}_i(t) \end{bmatrix} = \begin{bmatrix} \cos(\theta_i(t)) & 0 \\ \sin(\theta_i(t)) & 0 \\ 0 & 1 \end{bmatrix} u_i \tag{23}$$

where, $u_i = \left[v_i(t) \quad w_i(t)\right]^T$ is the control input for the system and $v_i \in \mathbb{R}$ and $w_i \in \mathbb{R}$ represent the translational and angular velocities of the robot i, respectively.

Denote the configuration of virtual robot i as $q_i^* = \left[p_i^* \quad \theta_i^*\right]^T \in \mathbb{R}^2 \times \mathbb{T}$. Then, the position of robot i can be mapped to its corresponding virtual robot's position as (15). Moreover, $\theta_i^* = \theta_i$ is defined w.r.t. the world frame. Thus, the virtual robot's kinematics can be derived as

$$\dot{q}_i^* = \dot{q}_i = \begin{bmatrix} \dot{x}_i^* \\ \dot{y}_i^* \\ \dot{\theta}_i^* \end{bmatrix} = \begin{bmatrix} \cos(\theta_i) & 0 \\ \sin(\theta_i) & 0 \\ 0 & 1 \end{bmatrix} u_i^* \tag{24}$$

where $u_i^* = \left[v_i^* \quad w_i^*\right]^T$ is the virtual control input for the systems.

Corollary 3.2. *Given Corollary 3.1, we can see that an equilibrium $D_i^{-1}\sum_{j\in\mathcal{N}_i}p_j^*D_i^{-1}$ is in the invariance set the virtual nonholonomic robot i to achieve position consensus in the virtual robots system or reach a desired formation on true robots system. Similarly, an equilibrium $D_i^{-1}\sum_{j\in\mathcal{N}_i}\theta_j^*D_i^{-1}$ is in the invariance set for reaching heading consensus in both the virtual and real system.*

The proof of the first part of the Corollary 3.2 is given in the proof of the Proposition 3.1. The proof of the second part of the Corollary 3.2 will be given below.

Proposition 3.2. *Given Assumption 2.1 and $\theta_i^* = \theta_i$, suppose the following control input is applied to each virtual and real agent*

$$\begin{aligned} w_i^* &= D_i^{-1}\sum_{j\in\mathcal{N}_i}(\theta_j^* - \theta_i^*)D_i^{-1} \\ &= \left(D_i^{-1}\sum_{j\in\mathcal{N}_i}\theta_j^*D_i^{-1}\right) - \theta_i^*, \end{aligned} \tag{25}$$

then, the virtual and real agents will reach heading consensus.

Proof. The closed-loop virtual system dynamics can be written compactly as

$$\dot{\theta}^* = -(L^d \otimes I_n)\theta^*(t) \tag{26}$$

where $w^* = \left[w_1^*, w_2^*, \ldots, w_N^*\right]^T \in \mathbb{R}^N$ and $\theta^* = \left[\theta_1^*, \theta_2^*, \ldots, \theta_N^*\right]^T \in \mathbb{R}^N$. The rest of the proof will be omitted since it is same as the proof of the Proposition 3.1. ■

However, nonholonomic mobile robots are governed by nonholonomic constraints. So we need to design a new control law to regulate each virtual nonholonomic robot's pose to a desired equilibrium or pose $q_{id} = \left[\left(D_i^{-1}\sum_{j\in\mathcal{N}_i}p_j^*D_i^{-1}\right)^T, D_i^{-1}\sum_{j\in\mathcal{N}_i}\theta_j^*D_i^{-1}\right]^T$. Then all virtual robots will converge to a common pose and the real robots will achieve the desired formation. Thus, the consensus problem can be considered as a pose regulation problem. To converge to the pose, a control law should be designed such that

$$\lim_{t\to\infty} q_{id} - q_i^* = 0. \tag{27}$$

The equivalent error ϵ_i is used to express $\left(q_{id} - q_i^*\right)$ in the robot's local coordinate frame

$$\begin{aligned} \epsilon_i = \begin{bmatrix}\epsilon_{x_i}\\ \epsilon_{y_i}\\ \epsilon_{\theta_i}\end{bmatrix} &= \begin{bmatrix}\cos(\theta_i) & \sin(\theta_i) & 0\\ -\sin(\theta_i) & \cos(\theta_i) & 0\\ 0 & 0 & 1\end{bmatrix}\left(q_{id} - q_i^*\right) \\ &= R(\theta_i)\tilde{q}_i. \end{aligned} \tag{28}$$

Moreover, the rotation matrix $R(\theta_i)$ is invertible, so $\epsilon_i \to 0$ if and only if $\tilde{q}_i \to 0$. Taking the derivative of (28) with the nonholonomic constraint, the error dynamics become [51]

$$\dot{\epsilon}_i = \begin{bmatrix}\dot{\epsilon}_{x_i}\\ \dot{\epsilon}_{y_i}\\ \dot{\epsilon}_{\theta_i}\end{bmatrix} = \begin{bmatrix}w_i^*\epsilon_{y_i} - v_i^* + v_{d_i}\cos(\epsilon_{\theta_i})\\ -w_i^*\epsilon_{x_i} + v_{d_i}\sin(\epsilon_{\theta_i})\\ -w_i^*\end{bmatrix}. \tag{29}$$

Proposition 3.3 (*Pose Coordination*). *Given Assumption 2.1, choose control inputs v_i^* and w_i^**

$$\begin{aligned} v_i^* &= v_{d_i}\cos(\epsilon_{\theta_i}) + k_x\epsilon_{x_i} \\ w_i^* &= k_y v_{d_i}\epsilon_{y_i}\frac{\sin(\epsilon_{\theta_i})}{\epsilon_{\theta_i}} + k_\theta\epsilon_{\theta_i} \end{aligned} \tag{30}$$

where k_x, k_y and k_θ are positive scalar gains, and the feed forward term v_{d_i} is given by

$$v_{d_i} = k_0\begin{cases}\exp(-\tau) & \text{if } \left|v_i^* - v_j^*\right| \geq \kappa \text{ and } i \neq j\\ \sigma(t) & \text{otherwise}\end{cases} \tag{31}$$

where $\sigma(\cdot) \in \mathbb{R}^+$ is a bump function, and k_0, τ and κ are tunable positive constant scalars. All agents will reach the pose coordination i.e., the desired formation and heading consensus simultaneously by applying control law (30) to each agent.

Remark 3.1 (*Bump Function*). A bump function $\sigma(t) : [0, \infty) \to [0, \mathbb{R}^+]$ is given by

$$\sigma(t) = \begin{cases}\exp\left(\dfrac{-\tau}{1 - \left(\frac{(t-t_0)}{n}\right)^2}\right) & \text{if } 0 < t_0 \leq t < n + t_0\\ 0 \quad \text{otherwise}\end{cases} \tag{32}$$

where t_0 and $n \in \mathbb{R}^+$ denote the time of the bump function is triggered and time before the bump function dies out, respectively. The function is both smooth and compactly supported. The function also has smooth derivative of any order, $\dot{\sigma}(t)$ is uniformly continuous, and $\ddot{\sigma}(t) \in L_\infty$.

Proof. Consider a Lyapunov function V as

$$V = \sum_{i=1}^{N}\frac{1}{2}\left(\epsilon_{x_i}^2 + \epsilon_{y_i}^2\right) + \frac{1}{2k_y}\epsilon_{\theta_i}^2 + \frac{1}{2}v_{d_i}^2. \tag{33}$$

The derivative of the Lyapunov function with the control inputs (30) is

$$\begin{aligned} \dot{V} &= \sum_{i=1}^{N}\epsilon_{x_i}\dot{\epsilon}_{x_i} + \epsilon_{y_i}\dot{\epsilon}_{y_i} + \frac{1}{k_y}\epsilon_{\theta_i}\dot{\epsilon}_{\theta_i} + v_{d_i}\dot{v}_{d_i} \\ &= \sum_{i=1}^{N}\epsilon_{x_i}(w_i^*\epsilon_{y_i} - v_i^* + v_{d_i}\cos(\epsilon_{\theta_i})) - \exp(-2\tau)\dot{\sigma}(t) \\ &\quad + \epsilon_{y_i}(-w_i^*\epsilon_{x_i} + v_{d_i}\sin(\epsilon_{\theta_i})) + \frac{1}{k_y}\epsilon_{\theta_i}(-w_i^*) \\ &= \sum_{i=1}^{N} -k_x\epsilon_{x_i}^2 - \frac{k_\theta}{k_y}\epsilon_{\theta_i}^2 - \exp(-2\tau)\dot{\sigma}(t) \leq 0. \end{aligned} \tag{34}$$

Since $V > 0$ and $\dot{V} \leq 0$, we have $V(t) \leq V(0) < \infty$. Thus, $V(t)$ is bounded, and so ϵ_{xi}, ϵ_{yi}, and ϵ_{θ_i} must be bounded also.

The boundedness of $V(t)$ implies that the terms $\epsilon_{x_i}, \epsilon_{y_i}, \epsilon_{\theta_i}, v_{d_i} \in L_\infty$. From (33) and (34), ϵ_{x_i} and $\epsilon_{\theta_i} \in L_2$. Based on the previous facts, (30) can be used to determine the control input $v_i^*, w_i^* \in L_\infty$. Consequently, from (29), we see $\dot{\epsilon}_{x_i}, \dot{\epsilon}_{y_i}, \dot{\epsilon}_{\theta_i} \in L_\infty$. Since $\dot{\epsilon}_{x_i}, \dot{\epsilon}_{y_i}, \dot{\epsilon}_{\theta_i}, \ddot{\sigma}(t) \in L_\infty$, then $\epsilon_{x_i}, \epsilon_{y_i}, \epsilon_{\theta_i}, \dot{\sigma}(t)$ are uniformly continuous. Based on the facts that $\epsilon_{x_i}, \epsilon_{\theta_i} \in L_\infty$ and that $\epsilon_{x_i}, \epsilon_{\theta_i} \in L_2$, Barbalat's lemma [52] can be employed to conclude that s's lemma [52] can be employed to conclude that

$$\lim_{t\to\infty} \epsilon_{x_i}, \epsilon_{\theta_i} = 0. \tag{35}$$

The result in (35) can be used in conjunction with the closed-loop dynamics for $\dot{\epsilon}_{y_i}$ given in (29), to determine that

$$\lim_{t\to\infty} \dot{\epsilon}_{y_i} = 0. \tag{36}$$

Substituting control input (30) to the third equation of (29)

$$\dot{\epsilon}_{\theta_i} = -v_{d_i}k_y\epsilon_{y_i}\frac{\sin(\epsilon_{\theta_i})}{\epsilon_{\theta_i}} - k_\theta\epsilon_{\theta_i}. \tag{37}$$

Based on the result in (35), the second term of (37) goes to zero as $t \to \infty$ and $\lim_{\epsilon_{\theta_i}\to 0}\frac{\sin(\epsilon_{\theta_i})}{\epsilon_{\theta_i}} = 1$. Therefore, since $v_{d_i} \geq 0$ and ϵ_{y_i} is uniformly continuous, and ϵ_{θ_i} has a finite limit as $t \to \infty$, the extended Barbalat's lemma [53] can be involved to show that

$$\lim_{t\to\infty} \dot{\epsilon}_{\theta_i} = 0 \text{ and } \lim_{t\to\infty} \epsilon_{y_i} = 0. \tag{38}$$

Substituting control input (30) to the first equation of (29)

$$\dot{\epsilon}_{x_i} = \left(v_{d_i} k_y \epsilon_{y_i} \frac{\sin(\epsilon_{\theta_i})}{\epsilon_{\theta_i}} + k_\theta \epsilon_{\theta_i}\right)\epsilon_{y_i} - k_x \epsilon_{x_i}. \tag{39}$$

Eq. (39) with the results in (35) and (38) can be used to conclude

$$\lim_{t\to\infty} \dot{\epsilon}_{x_i} = 0. \tag{40}$$

Then the control input (30) converges to $\lim_{t\to\infty} v_i^*(t) = v_{d_i}$ and $\lim_{t\to\infty} w_i^*(t) = 0$ since $\epsilon_i \to 0$. If $\left|v_i^* - v_j^*\right| < \kappa$ and $i \neq j$, $v_{d_i} = \sigma(t)$. Moreover, clearly, $\lim_{t\to(n+t_0)} v_{d_i} = 0$ in a finite time by definition of $\sigma(t)$ in (32).

Furthermore, Since $V \to \infty$ as $\left\|\epsilon_i, v_{d_i}\right\| \to \infty$, the Lyapunov function is radially unbounded. So we can conclude that the origin is globally asymptotically stable. In other words, $p_j^* = p_i^*$ and $\theta_j^* = \theta_i^*, \forall i, j (i \neq j) \in \{1, 2, \ldots, N\}$. Similarly, the multi-nonholonomic mobile robots system will converge to the desired formation and reach heading consensus-based on our analysis in Proposition 3.1 and its proof. ■

Remark 3.2 (*Localization*)**.** The necessary measurements to implement the proposed control law can be provided using a variety of on-board sensors, (e.g., the fusion of a camera and a lidar) or the fusion of GPS, INS and/or encoders, and using wireless communication to report each one's pose to the neighbors.

Remark 3.3 (*Common Orientation*)**.** The proposed approach also works without the knowledge of a global coordinate frame but with a common orientation axis. We can run heading consensus by itself to acquire a common orientation axis, such as measured by a magnetometer. The relative orientation to the neighbors can be estimated using vision based estimation algorithms.

3.3. Formation control and heading consensus with collision avoidance

Assumption 3.1. Assume that the initial distances and final formation distances between any all robots are larger than a pre-defined avoidance distance. In addition, we consider convex-type obstacles in this paper.

During formation control, the robots may collide with each other or other obstacles. Thus, we extend the proposed control law to include obstacle avoidance. Denote a robot sensor detection range as R, and a minimum acceptable distance to obstacles as r. If the robot i detects an obstacle within its avoidance region with a radius r, then a repulsive vector can be derived as

$$\vec{p}_{io} = p_i - p_o = [p_{io}^x, p_{io}^y]^T \in \mathbb{R}^2 \tag{41}$$

which points from the obstacle p_o to the ith robot. The obstacle p_o represents the nearest obstacle, which can be the nearest robot or the obstacle in the environment. The obstacle bearing angle θ_{io} w.r.t. the world frame is given as

$$\theta_{io} = \text{atan2}(-p_{io}^y, -p_{io}^x) \tag{42}$$

where $\text{atan2}(\cdot,\cdot) : \mathbb{R} \times \mathbb{R} \to \mathbb{T}$ is the quadrant-preserving arctangent function. Denote the angle $\tilde{\theta}_{io}$ as the relative angle between the robot heading and obstacle bearing measured in the local coordinate frame of the robot, i.e.,

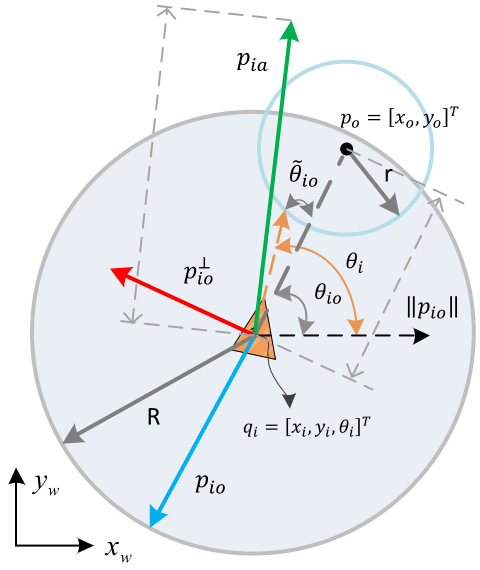

Fig. 3. The orange triangle represents the ith robot and the orange arrow is the heading direction with an orientation θ_i. The circular regions with radius R and r denote the sensor range and avoidance regions, respectively. The θ_{io} is a bearing angle between the robot and an obstacle. $\tilde{\theta}_{io}$ is the difference between the robot's heading and the bearing angle.

$$\tilde{\theta}_{io} = \theta_i - \theta_{io}. \tag{43}$$

The attractive vector is denoted as

$$\vec{p}_{ia} = D_i^{-1} \sum_{j\in N_i} p_j^* D_i^{-1} - p_i^*. \tag{44}$$

The geometry used to consider the avoidance problem is illustrated in Fig. 3.

Define a switching signal γ as

$$\gamma = \begin{cases} 0 & \text{if } \left|\tilde{\theta}_{io}\right| \geq \frac{\pi}{2} \text{ or } \|p_{io}\| > d_m \\ 1 & \text{otherwise} \end{cases} \tag{45}$$

where $d_m = \min(R, \frac{r}{\sin(|\tilde{\theta}_{io}|)})$.

The switching signal $\gamma = 1$ when the current robot trajectory may bring it within a distance r of an obstacle. In the presence of an obstacle, the robot should move along an avoidance vector $p_{io}^{\perp}$ that satisfies two conditions

$$\left\langle \vec{p}_{io}, \vec{p}_{io}^{\perp} \right\rangle = 0 \tag{46}$$

$$\left\langle \vec{p}_{ia}, \vec{p}_{io}^{\perp} \right\rangle \geq 0 \tag{47}$$

where $\langle\cdot\rangle$ denotes the inner product of two vectors. Denote the end point of the avoidance vector $\vec{p}_{io}^{\perp}$ as $p_{ic} = [x_{ic}, y_{ic}]^T \in \mathbb{R}^2$. Then, the desired orientation is given by

$$\theta_{ic} = \text{atan2}(y_{ic} - y_i, x_{ic} - x_i). \tag{48}$$

Denote that $q_{ic} = [p_{ic}^T, \theta_{ic}]^T$. Therefore, a unified pose is defined as

$$q_{iu} = (1-\gamma) q_{id} + \gamma q_{ic} \tag{49}$$

for each robot, and the unified velocity vector is given by

$$\vec{p}_{iu} = (1-\gamma)\vec{p}_{ia} + \gamma \vec{p}_{io}^{\perp} \tag{50}$$

which represents either the attractive vector or the repulsive vector.

The equivalent error ϵ_i is used to express $(q_{iu} - q_i^*)$ in the robot's local coordinate frame

$$\epsilon_i = \begin{bmatrix} \epsilon_{x_i} \\ \epsilon_{y_i} \\ \epsilon_{\theta_i} \end{bmatrix} = \begin{bmatrix} \cos(\theta_i) & \sin(\theta_i) & 0 \\ -\sin(\theta_i) & \cos(\theta_i) & 0 \\ 0 & 0 & 1 \end{bmatrix} (q_{iu} - q_i^*) = R(\theta_i)\tilde{q}_i. \tag{51}$$

Moreover, the rotation matrix $R(\theta_i)$ is invertible, so $\epsilon_i \to 0$ if and only if $\tilde{q}_i \to 0$.

Our system switches between achieving a desired formation along with heading consensus and obstacle avoidance, so we can consider our system as a hybrid switching system.

A general hybrid switching system can be formulated as

$$\dot{f}_q = \begin{cases} f_1 & \text{if } \gamma = 0 \\ f_2 & \text{if } \gamma = 1. \end{cases} \tag{52}$$

To establish stability we seek a common Lyapunov function for subsystem f_1 and f_2 [54]. Then the origin is asymptotically stable under switching signal γ.

Assumption 3.2. Assume that the magnitude of the avoidance vector is larger than the radius of the avoidance region $\left(\left\| \vec{p}_{io}^{\perp} \right\| > r \right)$.

Proposition 3.4. *Given Assumption 2.1, applying the control law (30), the pose of each agent will regulate in such a way that*

$$\lim_{t \to \infty} q_i - q_{iu} = 0, \forall i \in G. \tag{53}$$

Additionally, each agent will follow the velocity vector given in (50) and finally will converge to the desired pose q_{id}.

Proof. The Lyapunov function (33) is suitable as a common Lyapunov function. Applying the control law (30) to each robot will result in each robot's pose converge to its unified pose. Similarly, we also can conclude that the origin is globally asymptotically stable by Proof III.B.

Regardless of whether the robot is in either the obstacle-free region or the avoidance region, the dot product of the unified velocity vector and the attractive vector is greater than or equal to zero since we choose the attractive vector based on the conditions (46) and (47). The inner product of those two vectors is given as

$$\begin{aligned} \left\langle \vec{p}_{ia}, \vec{p}_{iu} \right\rangle &= \vec{p}_{ia}^{T} \left((1-\gamma)\vec{p}_{ia} + \gamma \vec{p}_{io}^{\perp} \right) \\ &= (1-\gamma)\vec{p}_{ia}^{T}\vec{p}_{ia} + \gamma \vec{p}_{ia}^{T}\vec{p}_{io}^{\perp} \\ &= \begin{cases} \vec{p}_{ia}^{T}\vec{p}_{ia} > 0 & \text{if } \gamma = 0 \\ \vec{p}_{ia}^{T}\vec{p}_{io}^{\perp} \geq 0 & \text{if } \gamma = 1. \end{cases} \end{aligned} \tag{54}$$

Clearly $\left\langle \vec{p}_{ia}, \vec{p}_{iu} \right\rangle \geq 0, \forall\gamma$, and $\left\langle \vec{p}_{ia}, \vec{p}_{iu} \right\rangle = 0$ iff $\tilde{\theta}_{io} = 0$. If some robots get deadlocked with an obstacle or other robot, velocities are zero such that the orientation consensus controller switches in, and it will rotate the robots and escape from a local minima [55,56]. Thus, an arbitrarily small rotation will make $\left\langle \vec{p}_{ia}, \vec{p}_{iu} \right\rangle > 0, \forall\gamma$.

- Case 1 (Obstacle-free region): It is obviously that each robot will move towards to its corresponding desired pose q_{id} in this region.
- Case 2 (Avoidance region): The robot will move towards to the temporary pose q_{ic} in the avoidance region. After reaching q_{ic}, the avoidance region will disappear and then the robot will move towards to the desired pose q_{id} again by Assumption 3.2. So clearly the robot cannot identically stay at the temporary pose q_{ic} and switch back to the obstacle-free region.

Therefore, the robot will finally converge to the desired pose q_{id}. In other words, we can see the virtual robot will reach consensus, and the true robots will achieve the desired formation and heading consensus by Proposition 3.3 and its proof. ■

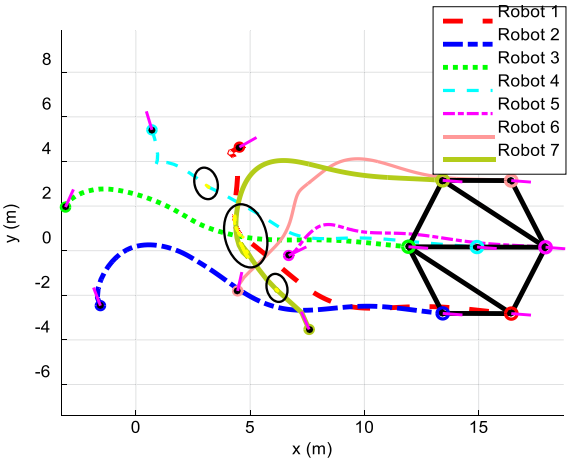

Fig. 4. Achieving desired formation along with heading consensus. The ellipses on the figure mean the corresponding robots are under collision avoidance mode. (For interpretation of the references to color in this figure legend, the reader is referred to the web version of this article.)

4. Simulations

Numerical simulations were created in MATLAB to demonstrate the efficacy and performance of the proposed formation control and heading consensus approach with collision avoidance strategy. Moreover, simulations were created by considering time-varying graph topologies and formation shapes. The robots were modeled as disks obeying the unicycle kinematic model. We set the sensing region with radius $R = 2.0$ m and the avoidance region with radius $r = 0.5$ m for each robot, and gains $k_x = 1$, $k_y = 1.5$ and $k_\theta = 1$.

4.1. Formation control and heading consensus for nonholonomic robots

In this simulation, seven nonholonomic mobile robots seek a desired formation as a final configurations of the seven robots shown in Fig. 4 and heading consensus while avoiding collision. The edges among the seven robots shown in Fig. 4 represent the network topology used in this simulation. The trajectories and initial and final headings are shown in Fig. 4. Figs. 5(a) and 5(b) verify that our approach successfully achieves the desired formation along with heading consensus smoothly (except when some robots are in the obstacle avoidance mode) and simultaneously. Note that the linear and angular velocities of all robots are tending to zero in Figs. 5(c) and 5(d) after the robots achieve the desired formation and heading consensus. However, we have observed that robots with numbers 1, 4, 6, and 7 lose smoothness in velocity when those robots enter obstacle avoidance mode, which are indicated by yellow trajectories in Fig. 4 during the task.

4.2. Formation control and heading consensus with switching topologies and formation shapes

Many systems cannot maintain a constant graph topology due to the failure of the communication or sensing link between robots

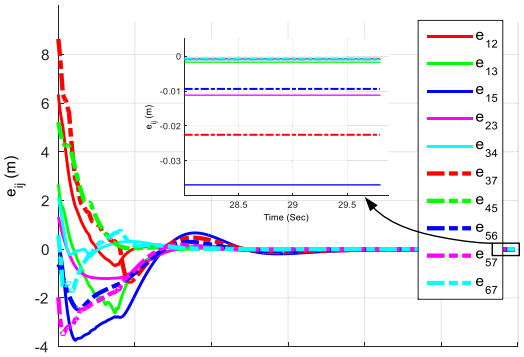

(a) Formation errors among robots converge to zero.

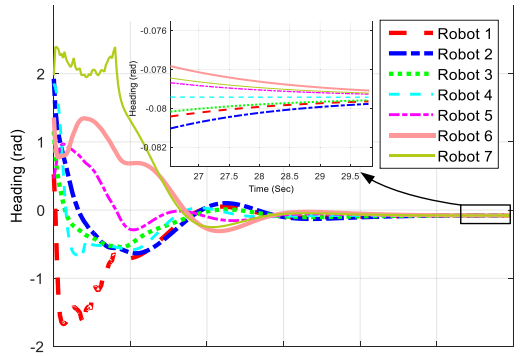

(b) Reach heading consensus.

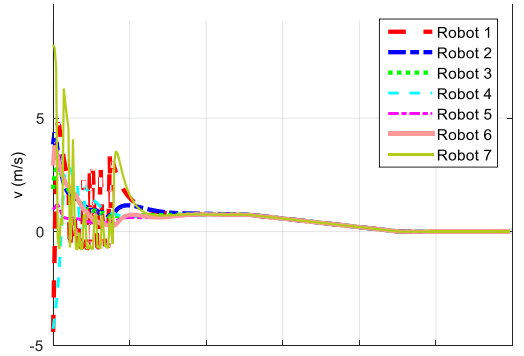

(c) Linear velocities converge to zero.

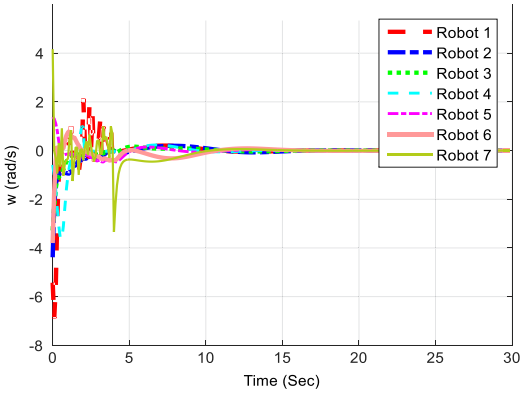

(d) Angular velocities converge to zero.

Fig. 5. Simulation results using five nonholonomic mobile robots.

or the displacement of the robot's position. Moreover, the robots may need to adjust the formation to fulfill different missions such as passing into narrow passage from a large space. Thus, it is necessary to investigate the situation of switching the shape of formation and the issue of changing the graph topology.

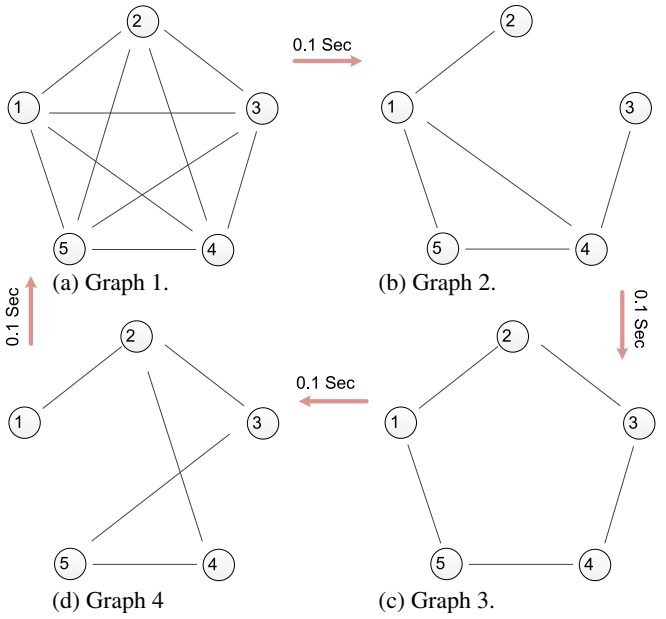

Fig. 6. A sequence of graph topologies used in simulation and switch in every 0.1 s.

We ran simulations using five robots to demonstrate that the system remains globally asymptotically stable during time-varying graph topologies and formation shapes. In this simulation, the network sampling rate is 10 Hz, and we repeatedly switch the graph topology through a sequence of graph topologies every 0.1 s as shown in Fig. 6. Moreover, we switch the formation shape to a straight line after 15 s. The trajectories over time are shown in Fig. 7. The results shown in Figs. 8 and 9 verified that the network connected five robots system achieve the desired formations and reach heading consensus smoothly. The results show that the switching topology does not noticeably affect smoothness of the control. Moreover, the non-smoothness in Fig. 8 near 15 s is due to a sudden changing on formation from a pentagon to a line. The apparent discontinuity in Fig. 9 around 17 s is due to a heading crossing π.

5. Experiments

To verify the effectiveness of the proposed approach, experiments have been conducted. The system configuration of the experiment is shown in Fig. 10. The poses of the robots are measured with a Vicon MX Motion Capture System, which has a sampling frequency of approximately 100 Hz. Using the Motion Capture System is similar to each robot having an accurate navigation system such as the fusion of GPS, IMU, and encoder, and then communicating its position to a set of neighbors via wireless communication. Note that the Vicon MX Motion Capture System can generally provide more accurate localization to the robots than any such combination of the sensors. The robots used in the experiment are four iRobot Create robots, which are nonholonomic mobile robots. The algorithms are implemented based on the Robot Operating System (ROS). To avoid collision during the motion, we added the collision avoidance controller with the novel switching signals given in (45). The sensing radius $R = 0.95$ m and the avoidance region with radius $r = 0.4$ m were used to design the switching surface, respectively.

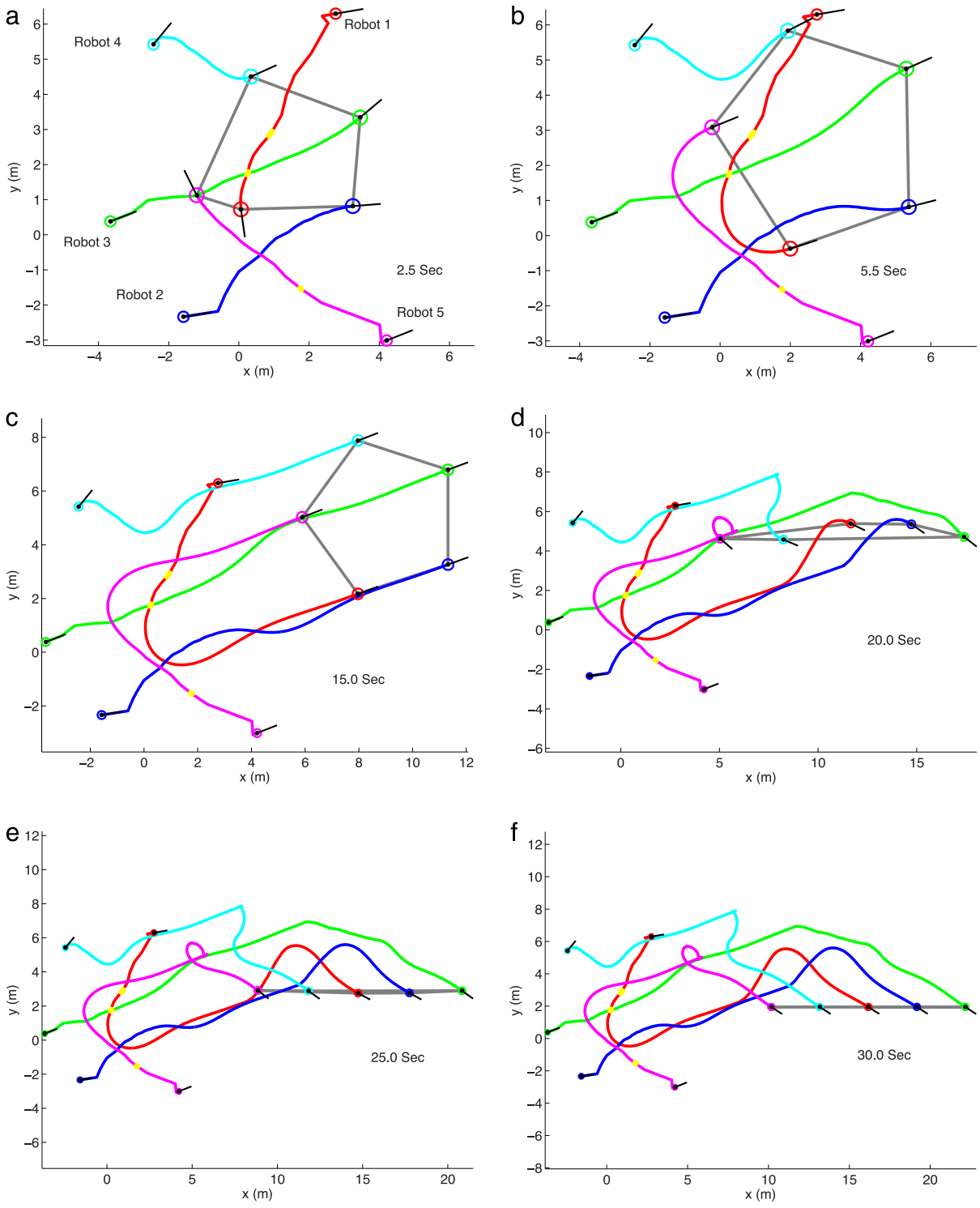

Fig. 7. The simulation result considering switching network topologies and formations. The ellipses on the subfigure (a) means the corresponding robots are under collision avoidance region.

In this experiment, we demonstrated that four robots achieved the desired formation and heading consensus simultaneously. A sequence of undirected graph topologies used in the experiment are illustrated in Fig. 11, and the sequence was updated every 1.0 s. The trajectories of the robots are shown in Fig. 12, and the yellow line on the trajectories indicates that the robot is in the avoidance mode. Furthermore, we observe that the formation errors converge to zero in Fig. 13(a), and as robots reach heading consensus in Fig. 13(b). The whole evolution took approximately 15 s, and the evolution speed depends on control gains. We also can observe that the linear and angular velocities decrease to zero along with achieving the desired formation and heading consensus, which are shown in Figs. 13(c) and 13(d). The discontinuities of linear and angular velocities in Figs. 13(c) and 13(d) indicate that the corresponding robot is in the collision avoidance mode.

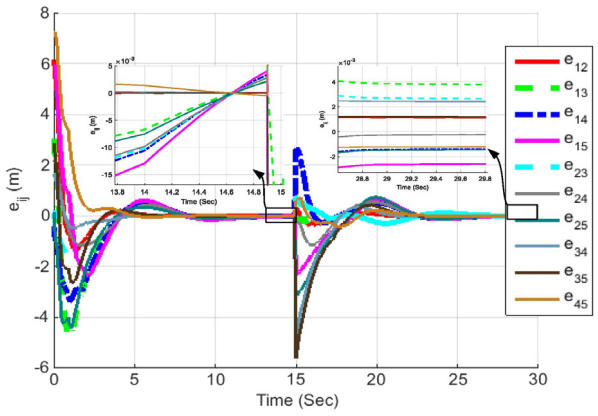

Fig. 8. Switching topology: formation errors among five nonholonomic mobile robots.

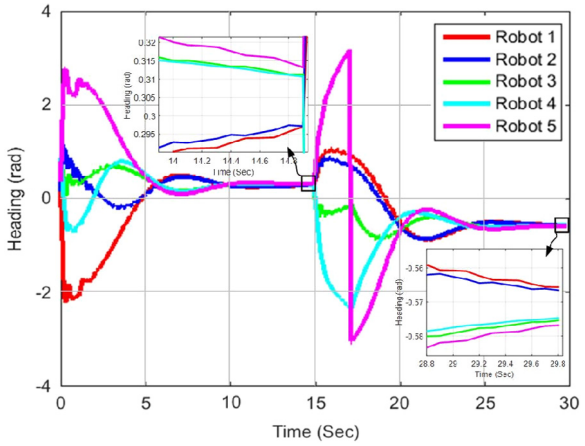

Fig. 9. Switching topology: the heading consensus is reached by five nonholonomic mobile robots.

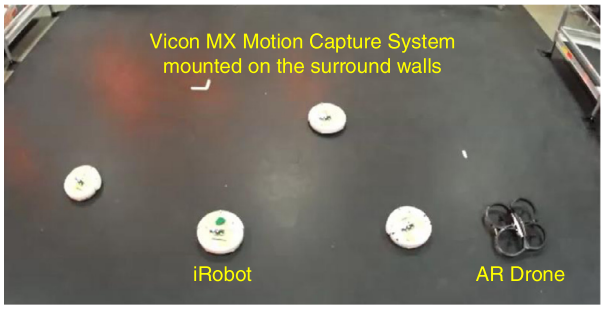

Fig. 10. Experimental setup.

6. Conclusion

In this paper, a novel decentralized control algorithm is proposed to address the problem of controlling multiple, network connected, nonholonomic mobile robots to achieve a desired formation along with the heading consensus. Note that for nonholonomic robots to execute motions while maintaining formation, the heading consensus must be achieved. Our approach employs a virtual graph that is isomorphic to the robots' graph such that the two graphs share same Laplacian and normalized Laplacian matrices. Moreover, the normalized Laplacian matrix-based design transforms the formation and heading consensus problem on $\mathbb{R}^2 \times \mathbb{T}$ to a pose regulation problem. Then a novel decentralized control law is designed to achieve consensus on the virtual graph and that same control inputs applied to the real robot systems will induce the multiple robot systems to the desired formation along with heading consensus. Collision avoidance is considered to ensure the safety during the motion. We prove the proposed control schemes are globally asymptotically stable. To verify the effectiveness of the proposed approach, several simulations and experiments have been conducted. The stability analysis under switching topologies and robustness to errors in pose measurement will be considered in our future work.

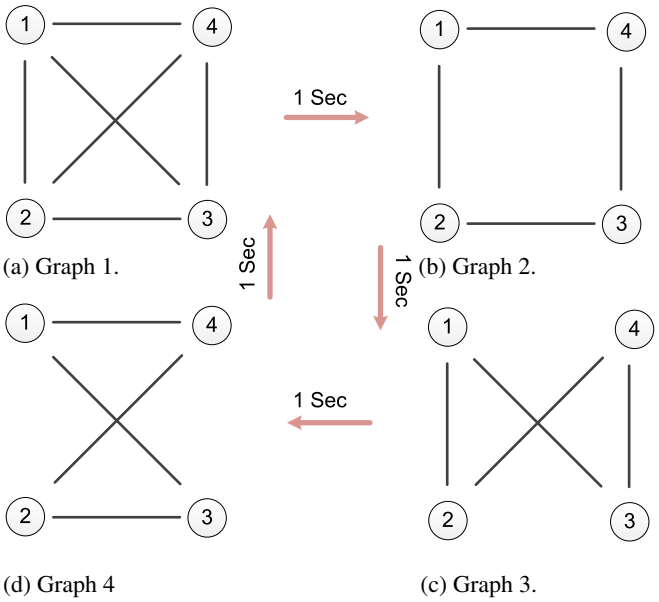

Fig. 11. A sequence of graph topologies used in the experiment that switches in every 1.0 s.

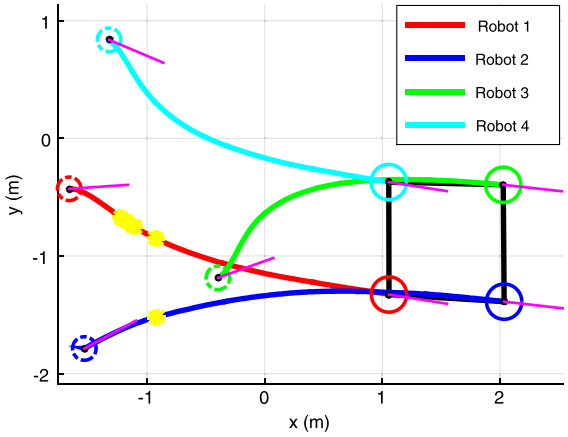

Fig. 12. Achieving desired formation along with heading consensus. The small and large circles represent the initial and final positions of robots, respectively. The yellow-dots on the figure mean the corresponding robots are under collision avoidance mode. (For interpretation of the references to color in this figure legend, the reader is referred to the web version of this article.)

Acknowledgment

This work was supported in part by DGIST R&D Program of the Ministry of Education, Science and Technology of Korea (15-BD-0101).

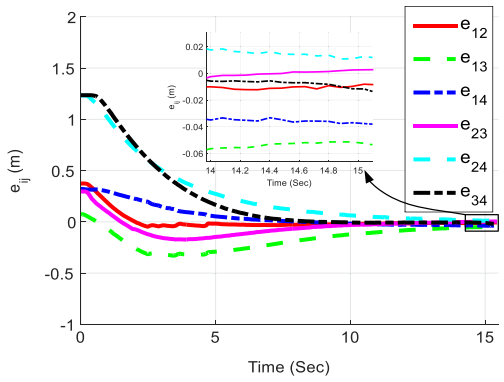

(a) Formation errors converge to zero.

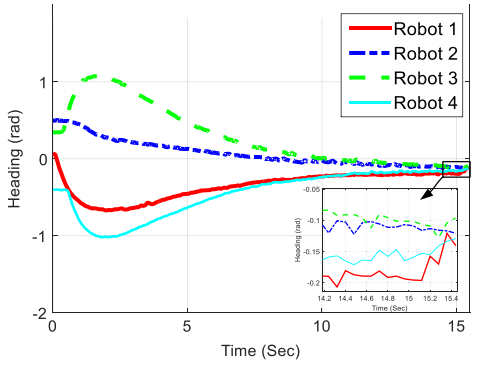

(b) Reach heading consensus.

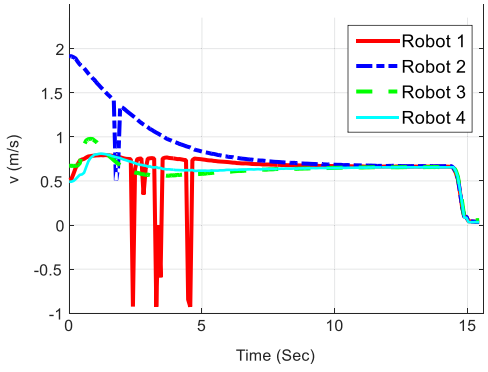

(c) Linear velocities of the robots.

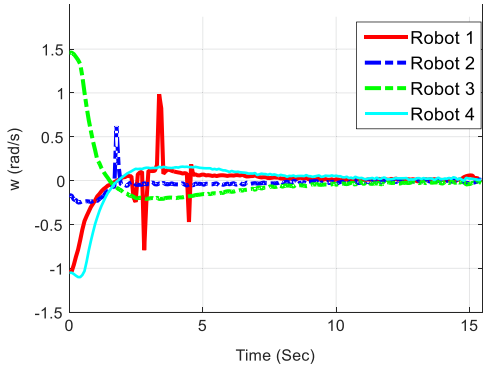

(d) Angular velocities of the robots.

Fig. 13. Experimental results including obstacle avoidance strategy. The discontinuities of linear and angular velocities indicate that the corresponding robot is in the collision avoidance mode. Yellow highlighted trajectories indicate the system was in obstacle avoidance mode. (For interpretation of the references to color in this figure legend, the reader is referred to the web version of this article.)

Appendix A. Supplementary data

Supplementary material related to this article can be found online at http://dx.doi.org/10.1016/j.robot.2017.05.008.

References

[1] N. Michael, J. Fink, V. Kumar, Cooperative manipulation and transportation with aerial robots, Auton. Robots 30 (1) (2011) 73–86.
[2] D. Mellinger, M. Shomin, N. Michael, V. Kumar, Cooperative grasping and transport using multiple quadrotors, in: Distributed Autonomous Robotic Systems, Springer, 2013, pp. 545–558.
[3] J.J. Acevedo, B.C. Arrue, I. Maza, A. Ollero, A decentralized algorithm for area surveillance missions using a team of aerial robots with different sensing capabilities, in: International Conference on Robotics and Automation, 2014, pp. 4735–4740.
[4] N. Noguchi, J. Will, J. Reid, Q. Zhang, Development of a master–slave robot system for farm operations, Comput. Electron. Agric. 44 (1) (2004) 1–19.
[5] A. Guillet, R. Lenain, B. Thuilot, P. Martinet, Adaptable robot formation control: Adaptive and predictive formation control of autonomous vehicles, IEEE Robot. Autom. Mag. (ISSN: 1070-9932) 21 (1) (2014) 28–39. http://dx.doi.org/10.1109/MRA.2013.2295946.
[6] D.W. Casbeer, D.B. Kingston, R.W. Beard, T.W. McLain, Cooperative forest fire surveillance using a team of small unmanned air vehicles, Int. J. Syst. Sci. 37 (6) (2006) 351–360.
[7] J. Zhou, Q. Hu, M.I. Friswell, Decentralized finite time attitude synchronization control of satellite formation flying, J. Guid. Control Dyn. 36 (1) (2012) 185–195.
[8] J.J. Acevedo, B.C. Arrue, I. Maza, A. Ollero, Cooperative large area surveillance with a team of aerial mobile robots for long endurance missions, J. Intell. Robot. Syst. 70 (1–4) (2013) 329–345.
[9] R. Olfati-Saber, R.M. Murray, Consensus problems in networks of agents with switching topology and time-delays, IEEE Trans. Automat. Control 49 (9) (2004) 1520–1533.
[10] L. Consolini, F. Morbidi, D. Prattichizzo, M. Tosques, Leader–follower formation control of nonholonomic mobile robots with input constraints, Automatica 44 (5) (2008) 1343–1349.
[11] K.D. Do, Formation tracking control of unicycle-type mobile robots with limited sensing ranges, IEEE Trans. Control Syst. Technol. 16 (3) (2008) 527–538.
[12] S. Mastellone, D.M. Stipanović, C.R. Graunke, K.A. Intlekofer, M.W. Spong, Formation control and collision avoidance for multi-agent non-holonomic systems: Theory and experiments, Int. J. Robot. Res. 27 (1) (2008) 107–126.
[13] K.D. Do, Output-feedback formation tracking control of unicycle-type mobile robots with limited sensing ranges, Robot. Auton. Syst. 57 (1) (2009) 34–47.
[14] M. Aranda, G. López-Nicolás, C. Sagüés, M.M. Zavlanos, Coordinate-free formation stabilization based on relative position measurements, Automatica 57 (2015) 11–20.
[15] A.-A. Agha-Mohammadi, S. Agarwal, A. Mahadevan, S. Chakravorty, D. Tomkins, J. Denny, N.M. Amato, Robust online belief space planning in changing environments: Application to physical mobile robots, in: IEEE International Conference on Robotics and Automation, 2014, pp. 149–156.
[16] X.L. Ai, J.Q. Yu, Y.B. Chen, F.Z. Chen, Y.C. Shen, Optimal formation control with limited communication for multi-unmanned aerial vehicle in an obstacle-laden environment, Proc. Inst. Mech. Eng. G (2016) p. 0954410016646599.
[17] T. Nägeli, J. Alonso-Mora, A. Domahidi, D. Rus, O. Hilliges, Real-time motion planning for aerial videography with dynamic obstacle avoidance and viewpoint optimization, IEEE Robot. Autom. Lett. (2017).
[18] D. Sun, A. Kleiner, B. Nebel, Behavior-based multi-robot collision avoidance, in: Robotics and Automation (ICRA), 2014 IEEE International Conference on, IEEE, 2014, pp. 1668–1673.
[19] L.G. Torres, A. Kuntz, H.B. Gilbert, P.J. Swaney, R.J. Hendrick, R.J. Webster, R. Alterovitz, A motion planning approach to automatic obstacle avoidance during concentric tube robot teleoperation, in: Robotics and Automation (ICRA), 2015 IEEE International Conference on, IEEE, 2015, pp. 2361–2367.
[20] M.A. Lewis, K.-H. Tan, High precision formation control of mobile robots using virtual structures, Auton. Robots 4 (4) (1997) 387–403.
[21] W. Ren, R. Beard, Decentralized scheme for spacecraft formation flying via the virtual structure approach, J. Guid. Control Dyn. 27 (1) (2004) 73–82.
[22] T.H. van den Broek, N. van de Wouw, H. Nijmeijer, Formation control of unicycle mobile robots: a virtual structure approach, in: Proceedings of the 48th IEEE Conference on Decision and Control Held Jointly with the 28th Chinese Control Conference, 2009, pp. 8328–8333.
[23] H. Lim, Y. Kang, J. Kim, C. Kim, Formation control of leader following unmanned ground vehicles using nonlinear model predictive control, in: IEEE/ASME International Conference on Advanced Intelligent Mechatronics, 2009, pp. 945–950.
[24] H.A. Poonawala, A.C. Satici, M.W. Spong, Leader-follower formation control of nonholonomic wheeled mobile robots using only position measurements, in: 2013 9th Asian Control Conference, 2013, pp. 1–6.

[25] C. Guo, J. Qin, Y. Ge, Y. Chen, Leader-follower and cascade system based formation control of nonholonomic intelligent vehicles, in: The 26th Chinese Control and Decision Conference, 2014, pp. 3931–3935.
[26] M. Ji, M. Egerstedt, Distributed coordination control of multiagent systems while preserving connectedness, IEEE Trans. Robot. (ISSN: 1552-3098) 23 (4) (2007) 693–703. http://dx.doi.org/10.1109/TRO.2007.900638.
[27] D. Zelazo, A. Franchi, F. Allgöwer, H.H. Bülthoff, P.R. Giordano, Rigidity maintenance control for multi-robot systems, Robot. Sci. Syst. (2012) 473–480.
[28] R. Olfati-Saber, J.A. Fax, R.M. Murray, Consensus and cooperation in networked multi-agent systems, Proc. IEEE 95 (1) (2007) 215–233.
[29] W. Ren, N. Sorensen, Distributed coordination architecture for multi-robot formation control, Robot. Auton. Syst. 56 (4) (2008) 324–333.
[30] J.R. Lawton, R.W. Beard, B.J. Young, A decentralized approach to formation maneuvers, IEEE Trans. Robot. Autom. 19 (6) (2003) 933–941.
[31] A. Franchi, P.R. Giordano, Decentralized control of parallel rigid formations with direction constraints and bearing measurements, in: IEEE 51st Annual Conference on Decision and Control, 2012, pp. 5310–5317.
[32] S. Zhao, F. Lin, K. Peng, B.M. Chen, T.H. Lee, Finite-time stabilisation of cyclic formations using bearing-only measurements, Internat. J. Control 87 (4) (2014) 715–727.
[33] G.C. Calafiore, L. Carlone, M. Wei, Position estimation from relative distance measurements in multi-agents formations, in: Control & Automation (MED), 2010 18th Mediterranean Conference on, 2010, pp. 148–153.
[34] C.-F. Chang, C.-C. Tsai, Formation stabilization of nonholonomic multi-robot systems using relative distance measurements, in: IEEE International Conference on System Science and Engineering, 2014, pp. 1–6.
[35] E. Montijano, D. Zhou, M. Schwager, C. Sagues, Distributed formation control without a global reference frame, in: Proc. of the American Control Conference, ACC 14, 2014, pp. 3862–3867.
[36] J.A. Fax, R.M. Murray, Information flow and cooperative control of vehicle formations, IEEE Trans. Automat. Control 49 (9) (2004) 1465–1476.
[37] W. Ren, Collective motion from consensus with Cartesian coordinate coupling-Part I: Single-integrator kinematics, in: 47th IEEE Conference on Decision and Control, 2008, pp. 1006–1011.
[38] W. Ren, Consensus based formation control strategies for multi-vehicle systems, in: American Control Conference, 2006, pp. 4237–4242.
[39] R.W. Brockett et al., Asymptotic Stability and Feedback Stabilization, 1983.
[40] K.D. Listmann, M.V. Masalawala, J. Adamy, Consensus for formation control of nonholonomic mobile robots, in: IEEE International Conference on Robotics and Automation, 2009, pp. 3886–3891.
[41] W. Dong, Flocking of multiple mobile robots based on backstepping, IEEE Trans. Syst. Man Cybern. B 41 (2) (2011) 414–424.
[42] K. Cao, B. Jiang, D. Yue, Distributed consensus of multiple nonholonomic mobile robots, IEEE/CAA J. Autom. Sin. 1 (2) (2014) 162–170.
[43] H.G. Tanner, A. Jadbabaie, G.J. Pappas, Flocking in teams of nonholonomic agents, in: Cooperative Control, Springer, 2005, pp. 229–239.
[44] N. Moshtagh, A. Jadbabaie, Distributed geodesic control laws for flocking of nonholonomic agents, IEEE Trans. Automat. Control 52 (4) (2007) 681–686.
[45] H. Hu, S.Y. Yoon, Z. Lin, Flocking of wheeled vehicles in the presence of large communication delay through a potential functional approach, in: 52nd IEEE Conference on Decision and Control, 2013, pp. 3529–3534.
[46] J. Jin, Y.-G. Kim, S.-G. Wee, N. Gans, Consensus based attractive vector approach for formation control of nonholonomic mobile robots, in: 2015 IEEE International Conference on Advanced Intelligent Mechatronics, AIM, 2015, pp. 977–983.
[47] W. Ren, On consensus algorithms for double-integrator dynamics, IEEE Trans. Automat. Control 53 (6) (2008) 1503–1509.
[48] N. Biggs, Algebraic Graph Theory, Cambridge university press, 1993.
[49] A.C. Satici, H. Poonawala, H. Eckert, M.W. Spong, Connectivity preserving formation control with collision avoidance for nonholonomic wheeled mobile robots, in: 2013 IEEE/RSJ International Conference on Intelligent Robots and Systems, 2013, pp. 5080–5086.
[50] G. Klancar, I. Skrjanc, Tracking-error model-based predictive control for mobile robots in real time, Robot. Auton. Syst. 55 (2007) 460–469.
[51] Y. Kanayama, Y. Kimura, F. Miyazaki, T. Noguchi, A stable tracking control method for an autonomous mobile robot, in: IEEE International Conference on Robotics and Automation, 1990, pp. 384–389.
[52] J.-J.E. Slotine, W. Li, et al., Applied Nonlinear Control, vol. 199, Prentice-Hall Englewood Cliffs, NJ, 1991.
[53] Y. Fang, W.E. Dixon, D.M. Dawson, P. Chawda, Homography-based visual servo regulation of mobile robots, IEEE Trans. Syst. Man Cybern. B 35 (5) (2005) 1041–1050.
[54] D. Liberzon, Switching in Systems and Control, Birkhauser, 2003.
[55] J. Jin, A. Green, N. Gans, A stable switched-system approach to obstacle avoidance for mobile robots in SE (2), in: 2014 IEEE/RSJ International Conference on Intelligent Robots and Systems, 2014, pp. 1533–1539.
[56] J. Jin, Y.-G. Kim, S.-G. Wee, N. Gans, Decentralized cooperative mean approach to collision avoidance for nonholonomic mobile robots, in: 2015 IEEE International Conference on Robotics and Automation, ICRA, 2015, pp. 35–41.

Jingfu Jin received his M.S. degree in electrical and computer engineering from Korea University, in 2010 and his Ph.D. in electrical engineering from the University of Texas at Dallas. He is currently an automated driving software engineering at General Motors. His research interests include Robotics, with focus on autonomous vehicles, multi-robot systems, and vision-based control and estimation.

Dr. Gans received the M.S. in electrical and computer engineering and his Ph.D. in systems and entrepreneurial engineering from the University of Illinois at Urbana–Champaign in 2002 and 2005, respectively. He is currently a Clinical Associate Professor at The University of Texas at Dallas. His research interests include nonlinear and adaptive control and optimization, with foci on vision-based control and estimation, robotics and autonomous vehicles.